NISTIR 6481

Molecular Dynamics Study of Tethered Chains

Raymond D. Mountain

U.S. DEPARTMENT OF COMMERCE
Technology Administration
Physical and Chemical Properties Division
100 Bureau Drive Stop 8380
National Institute of Standards
and Technology
Gaithersburg, MD 20899-8380 USA

Joseph B. Hubbard
Curtis W. Meuse
Vernon Simmons

U.S. DEPARTMENT OF COMMERCE
Technology Administration
Biotechnology Division
100 Bureau Drive Stop 8313
National Institute of Standards
and Technology
Gaithersburg, MD 20899-8313 USA

NIST
National Institute of Standards and Technology
Technology Administration
U.S. Department of Commerce

NISTIR 6481

Molecular Dynamics Study of Tethered Chains

Raymond D. Mountain

U.S. DEPARTMENT OF COMMERCE
Technology Administration
Physical and Chemical Properties Division
100 Bureau Drive Stop 8380
National Institute of Standards
and Technology
Gaithersburg, MD 20899-8380 USA

Joseph B. Hubbard
Curtis W. Meuse
Vernon Simmons

U.S. DEPARTMENT OF COMMERCE
Technology Administration
Biotechnology Division
100 Bureau Drive Stop 8313
National Institute of Standards
and Technology
Gaithersburg, MD 20899-8313 USA

March 2000

U.S. DEPARTMENT OF COMMERCE
William M. Daley, Secretary

TECHNOLOGY ADMINISTRATION
Dr. Cheryl L. Shavers, Under Secretary
of Commerce for Technology

NATIONAL INSTITUTE OF STANDARDS
AND TECHNOLOGY
Raymond G. Kammer, Director

Molecular dynamics study of tethered chains *

Raymond D. Mountain
Physical and Chemical Properties Division
100 Bureau Drive Stop 8380
National Institute of Standards and Technology
Gaithersburg, MD 20899-8380 USA

and

Joseph B. Hubbard, Curtis W. Meuse, and Vernon Simmons
Biotechnology Division
100 Bureau Drive Stop 8313
National Institute of Standards and Technology
Gaithersburg, MD 20899-8313 USA

Abstract: The results of a series of molecular dynamics simulations of monolayer films formed by tethered, long chain molecules (octadecanthiol) are discussed. The emphasis is on the structure of the chains. The density profiles, the distribution of *gauche* defects along the chains, and two orientation measures are described. Where possible, the connections with experimental probes of such films are mentioned.

1. Introduction

The characterization of the "surface" presented by a monolayer of long chain molecules tethered to a substrate is of interest in several areas of science. Here we discuss the results of a molecular dynamics simulation based examination of monolayers consisting of linear chains containing 19 nodes/sites. The particular configurations examined were selected to satisfy two rather different interests. The first interest is in the characterization of the "surface" presented by the monolayer formed by the untethered ends of the chains. Here, the chain molecules are closely packed on the substrate and are relatively free to translate along the substrate. The second interest is the role the monolayer plays in Reversed Phase Liquid Chromatography (RPLC). For this application, the chains are not closely packed and are rigidly tethered to specific locations on the substrate. In a future publication we will present a detailed molecular dynamics analysis of the behavior of shorter chains tethered to a surface.

Octadecanthiol monolayers on gold surfaces are one of the most studied examples of surface tethered chains. A variety of techniques including ellipsometry, electrochemistry, infrared spectroscopy, grazing incidence X- ray diffraction, scanning tunneling microscopy, and molecular dynamics simulations have been utilized to characterize the structure of octadecanethiol monolayers on Au(111) surfaces. Ellipsometry reveals that octadecanethiol monolayers are 2.3 nm thick.[1, 2] Electrochemistry reveals that octadecanethiol monolayers have an apparent fraction of the electrode surface of less than $6x10^{-6}$ which is deficient in the current blocking monolayer.[1, 3] Electron diffraction reveals that octadecanethiol

monolayers adopt a c(4x2) superlattice of a $\sqrt{3} \times \sqrt{3}R30°$ hexagonal lattice.[4, 3, 5, 6] The infrared reflection spectrum of an octadecanethiol monolayer on gold reveals that the asymmetric CH_2 stretching mode, $\nu_a(CH_2)$, is at 2917 cm^{-1} which corresponds with that of the bulk crystalline phase (2918 cm^{-1}).[1] Electromagnetic wave theory calculations of infrared reflection spectra reveal that the tilt angle of octadecanethiol on gold using a two chain model is 27° and that the two chains are twisted at 50° and 48° respectively so that the backbone planes of the two chains make an angle of 82°. This model further reveals that the fraction of terminal *gauche* CH_3 groups is 0.45±0.10.[7, 8] Low temperature IR reflection data of octadecanethiol monolayers on Au(111) surfaces yields a best fit with a single chain model with the chains tilted at 24° and twisted at 46°. This result is consistent with the small factor splitting of the d-mode known to occur in orthorhomibic crystals of n-alkane chains.[9] Grazing incidence X-ray diffraction indicates that octadecanethiol monolayers are 2.2 nm thick and the chains are tilted at an angle of 30.3°±0.5°. In order to achieve a c(4x2) superlattice of a $\sqrt{3}\times\sqrt{3}R30°$ hexagonal lattice, the chains have undergone a 4% reduction in the next nearest neighbor distance.[10, 5, 11] Recent studies of the structure of hexadecanethiol and octadecanethiol monolayers using infrared spectroscopy reveal slightly different values for the tilt, twist and fraction of terminal *gauche* groups. While the values for the tilt angles were different, -21° and -30°, respectively, both found best fits for single chain models with twist angles of 50° and 0.23–0.27±0.12 fraction of terminal *gauche* groups.[12, 13]

Previous molecular dynamics simulations have predicted that hexadecanethiol monolayers have a thickness of 2.0 nm and a tilt angle of between 20° and 30°, consistent with experiments. [14] However they have had difficulty predicting the fraction of *gauche* conformations consistent with experiment, predicting between 0.011 and 0.112. Further molecular dynamics simulations of the effects of temperature on the structure of hexadecanethiol monolayers showed a two site distribution of twist angles peaked near ± 97° which does not agree with 45°–50° determined from the IR data. They attribute this effect to the united atom approximation in their model.[15] An all-atoms molecular dynamics simulation of pentadecanethiol monolayers favors a herringbone structure with two chains per unit cell unlike the four chains per unit cell observed x-ray diffraction and scanning tunneling microscopy. [10, 16, 17] Using 90-100 chains, at room temperature, the simulations found a tilt angle of 30° and a twist angle of 50°, consistent with infrared experiments.[18]

The model for the chains and the surface employed here are discussed in Section 2 along with the details of the molecular dynamics simulation methods used in this study. The results of these simulations are discussed in Sections 3 and 4. Section 5 contains some summary observations.

2. Model details

A series of simulations have been made of a system of 225 linear chain molecules tethered to a smooth surface. Each chain consists of a "thiol" site that is strongly bound to the surface, followed by 17 CH_2 united atom sites, and terminated by one CH_3 united atom site. Figure 1 shows a single chain in an all *trans* configuration tilted at an angle of about 30° from the z-axis. The z-axis is normal to the substrate. The thiol site is indicated by

a large filled circle and is referred to as site number 1. Sites 2 through 18 are CH_2 united atom sites indicated by small shaded circles. Site 19 is the terminal methyl united atom site and is indicated as the small filled circle. The bonds between adjacent sites where torsion motions are possible are indicated by bold lines.

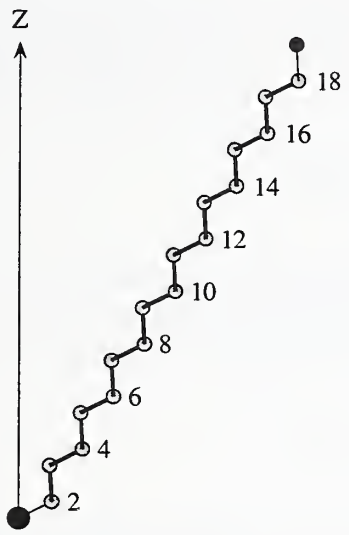

Figure 1. A single chain molecule containing 19 sites in an all *trans* configuration.

The properties of linear alkanethiol chains forming a (partial) monolayer on a surface are estimated using a molecular model. The molecules are represented in terms of a united atom, site-site interaction model for the chains. A "site" is a point where the force is applied. For the model considered here, a site corresponds to a carbon or sulfur atom position. This type of model for linear alkanes has been shown to provide satisfactory descriptions of several properties.[19] However, the parameters for the alkanethiol model are different from the corresponding parameters for alkanes as the former are purely empirical models. It is necessary to introduce molecule-surface interactions that maintain the monolayer. The interactions are divided into intramolecular terms, intermolecular terms, and surface-atom interaction terms.

Potentials

The intramolecular interaction,[14] V_{intra}, consists of four parts,

$$V_{intra} = V_2 + V_3 + V_4 + V_5.$$

The parameters in each term depend on the species of the sites entering the interaction, although this is not explicitly indicated here in order to avoid cluttering the notation. There are three species in the model; the thiol group, the CH_2 group, and the CH_3 group. Each group is treated as a single "atom" with the appropriate mass, hence the term united

atom model. In this report, the term "atom" is to be interpreted as "united-atom". This means that there are several values possible for each of the parameters. The specific values for the parameters are listed in several tables found in the appendix. The V_2 term contains the harmonic stretching interactions between bonded neighbors,

$$V_2 = \frac{1}{2}\sum_{i=1}^{N-1} \gamma_2 (r_{ij} - d_0)^2,$$

where $j = i+1$ and N is the number of atoms in a chain. The parameters for the stretching interaction are γ_2 and d_0. The V_3 term contains the harmonic bending interactions that involve adjacent triples of sites,

$$V_3 = \frac{1}{2}\sum_{i=1}^{N-2} \gamma_3 (\theta_{ijk} - \theta_0)^2,$$

$j = i+1$, $k = i+2$, and θ_{ijk} is the angle at site j subtended by sites i and k. The parameters for the bending interaction are γ_3 and θ_0. The V_4 term contains the torsion interactions that involves adjacent quadruples of sites,[20]

$$V_4 = \sum_{i=1}^{N-3} \sum_{l=0,5} C_l \cos^l(\phi)$$

where ϕ is the dihedral angle between the planes defined by the four sites and the C_l's are the parameters for the torsion interactions. The bonds where torsion rotations are possible are shown as heavy dark lines in Figure. 1.

The V_5 term describes the Lennard-Jones interactions between sites separated by three or more sites,

$$V_5 = \sum_{j=1}^{N-4} \sum_{k=j+4}^{N} V_{LJ}(r_{jk}).$$

The Lennard-Jones potential has the form

$$V_{LJ}(r) = 4\epsilon\left[\left(\frac{\sigma}{r}\right)^{12} - \left(\frac{\sigma}{r}\right)^{6}\right],$$

with energy depth and range parameters ϵ and σ, respectively.

The torsion and Lennard-Jones potentials are shown in Figure 2.

The intermolecular interactions are determined using the same Lennard-Jones potential that acts between intramolecular sites except that it acts between sites on distinct chain molecules.

The surface interaction introduced by Hautman and Klein[14] is a 12-3 surface potential of the form,

$$V_{surface}(z) = \frac{C_{12}}{(z - z_0)^{12}} - \frac{C_3}{(z - z_0)^3}.$$

Figure 2. The torsion potential is shown on the left, in units of kelvins. The parameters are those found in Table 3 below. The Lennard-Jones potential is shown on the right in units of the parameter ϵ.

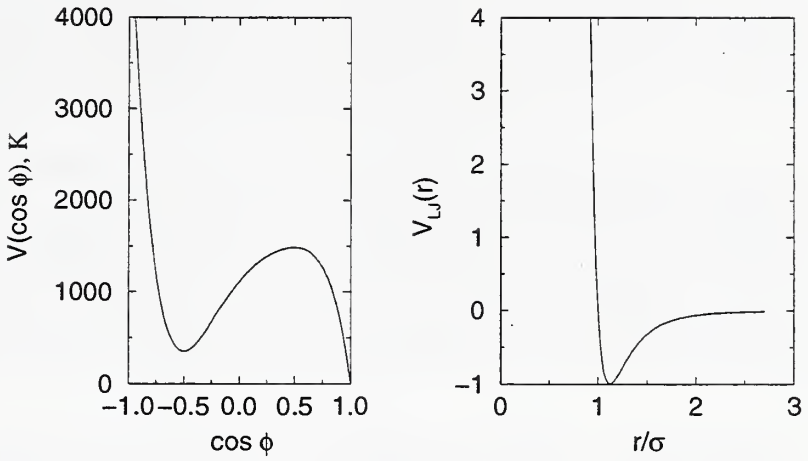

Figure 3. The surface potentials are shown here using the parameters from Table 4. The potential for the CH_3 sites is represented by the solid line, the potential for the CH_2 sites is represented by the short dashed line, and the potential for the thiol sites, *reduced by a factor of 20*, is represented by the long dashed line at the left side of the figure.

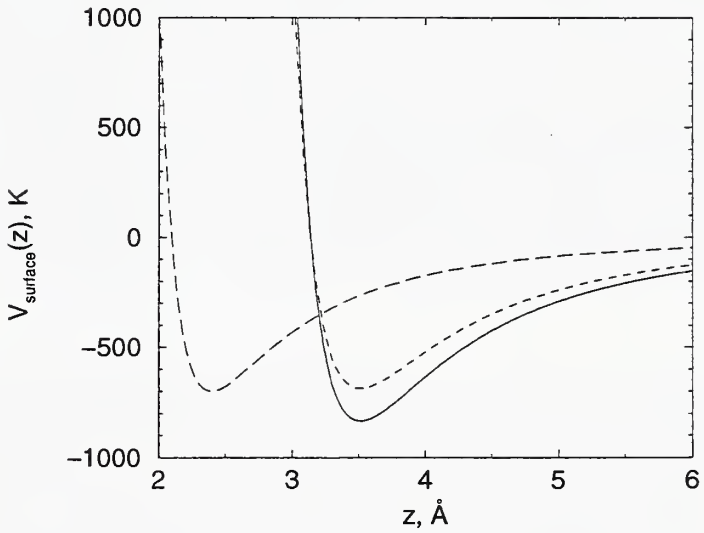

The interaction of each site in the chain depends on the distance of the site above the surface. The surface is otherwise unstructured. The surface interactions are shown in Figure 3. The introduction of surface structure is straightforward[21] but discussion of it is beyond the scope of this report.

Simulation details

The equations of motion resulting from these interaction potentials were integrated using an iterated form of the Beeman algorithm[22] with a time step of 1 fs. Periodic boundary conditions were imposed in the x- and y-directions, but not in the z-direction which is normal to the plane of the substrate to which the chains were tethered.

The initial conditions for the simulations, where free translation along the surface was allowed, had the chains arranged on a square lattice. These cases will be called the free translation cases. Three different packing densities were examined. The first has a high density of 4.655 chains/nm^2 (or 21.5Å^2/molecule), the second has a lower density of 3.605 chains/nm^2 (27.7Å^2/molecule), and the third has a density appropriate for RPCL columns of 2.504 chains/nm^2 (40.0Å^2/molecule). Subsequently these cases will be labeled C1, C2, and C3 respectively.

Two additional cases were examined for the density of 2.504 chains/nm^2. In these simulations the chains were not allowed to translate along the surface. The initial conditions were generated by placing the thiol sites at random positions on the surface subject to the condition that the minimum distance between thiol sites was greater than 0.442 nm. This condition was chosen to avoid overlaping chain configurations. The thiol sites were not permitted to move from these initial positions and the motions of the CH_2 and CH_3 sites were restricted as a result. These cases will be called the bound cases. Two distinct initial conditions were generated. Subsequently these simulations will be labeled C4 and C5.

For each case simulated, a series of stabilization runs were performed before a production run of 100 ps duration was made. During the stabilization runs, the chains developed a tilt relative to the substrate normal and some fraction of *gauche* defects. For the cases C1, C2, and C3, the thiol sites moved into an approximately hexagonal arrangement on the substrate with the amount of hexagonal order of the thiol sites decreasing as the density decreased. Unless otherwise stated, all simulations were for a temperature of close to 300 K.

A time series record of *trans-gauche* interconversions for the case C1 is shown in Fig. 4. The solid curve (middle line) is for the bond between sites 2 and 3, the line at the bottom of the figure is for the bond between sites 9 and 10, and the line at the top of the figure is for the bond between sites 17 and 18. These are averages over the 225 chains in the system. These histories are sufficiently stationary over 100 ps to indicate that we are sampling from a system of fully equilibrated chains. Also, the high frequency of interconversion events indicates that this system is dynamically very active. These curves capture the essence of the full set of histories for all of the cases C1–C3.

Several properties of these monolayers were monitored during the simulations. The first is the number density profile as a function of the distance above the substrate. The tilt angle distribution of the chains, $P(\cos\theta)$, was obtained by determining the cosine of the angle formed between the z-axis and the vector from site 1 to site 19. The fraction, f_G, of *gauche* defects for each of the bonds where torsion motion is possible was determined. A *gauche* defect was said to exist if the torsion angle, ϕ, was greater than 66°, the position

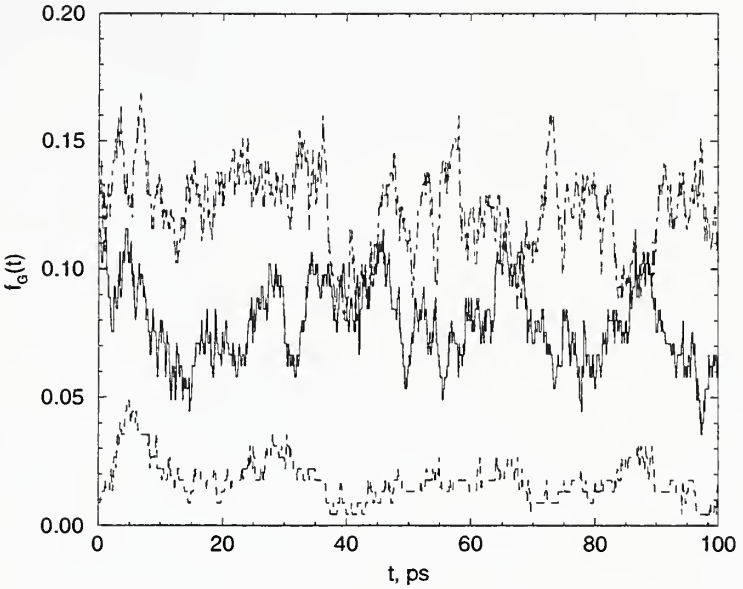

Figure 4. Time series for f_G, the fraction of *gauche* defects per bond, for case C1 are shown for three bonds as described in the text.

of the maximum in the torsion potential shown in Fig. 2. Finally, the order parameter,

$$S_2 = \frac{1}{2}\langle 3\cos^2\psi_j - 1\rangle,$$

was generated for each site. Here ψ_j is the angle formed between the z-axis and the vector between site *j-1* and site *j+1*. The discussion of the membranes in the next two sections will utilize these quantities.

3. Results, free translation

The density profiles are shown in Fig. 5. The highest surface packing density exhibits the most ordered z-projected density profile, with pronounced oscillations near the surface extending to a smooth profile as the terminal methyl is approached. Note that the layer thickness as given by the termination positions of these profiles is remarkably insensitive to the packing density. The range of 2.2–2.4 nm is in accord with the ellipsometrically determined value of 2.3 nm for the high density system.[1, 2] This thickness determination is consistent with the average position of the methyl group for case C1, namely 2.21±0.12 nm. The average positions of the methyl groups for the lower density cases are significantly smaller than the termination positions, namely 1.80±0.35 nm, and 1.54±0.61 nm for cases C2 and C3 respectively. This is a reflection of the higher degree of disorder in the lower density systems.

The overall tilt angle distributions are shown in Fig. 6. The sulfur-terminal methyl tilt angle distribution exhibits a pronounced broadening as the density changes from the highest to the lowest density, eventually developing several distinct maxima as the chains collapse onto the surface and overlap one another. Note that the principal minimum tilt angle is actually somewhat larger for C2 than for the lowest density C3 whereas the average tilt

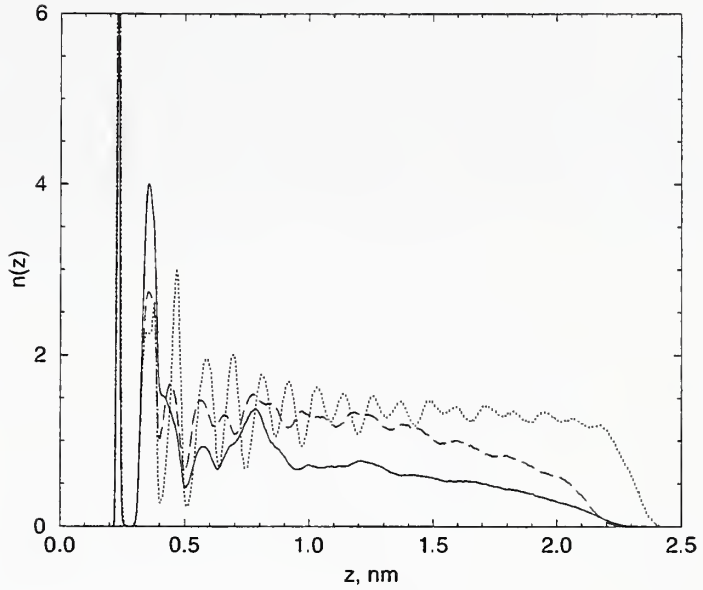

Figure 5. The density profiles for the three cases with free translation are displayed. The dotted line is for C1, the dashed line is for C2, and the solid line is for C3.

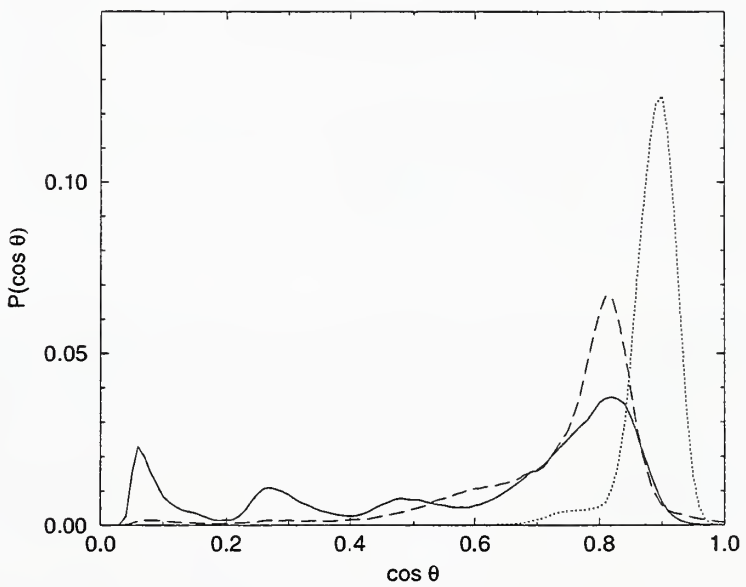

Figure 6. The tilt angle distributions for the three cases with free translation are displayed. The dotted line is for C1, the dashed line is for C2, and the solid line is for C3.

at density C2 is considerably less than that for C3 so one must take the entire angular distribution into consideration when considering tilt.

The fraction of *gauche* defects, f_G, for each bond torsion is shown in Fig. 7. The average fraction of *gauche* defects is largest at the two lowest packing densities; moreover, these defects appear to be concentrated at both the sulfur and methyl terminated ends of the chains. Note also that the chain interior makes a significant contribution to the total

number of *gauche* defects. These observations are in contradiction to the accepted practice employed in the infared spectroscopic analysis which is based on the assumption that all *gauche* defects are localized at the terminal methyl ends of the chains.[7, 8] The average number of *gauche* defects per chain is significantly larger than that reported by Klein *et al.* However a direct comparison between the two simulations cannot be made as the Klein group used 22-carbon atom chains at a density of 4.90 chains/nm^2, whereas in our high density simulation there are 18-carbon atom chains the and a slightly lower surface density of 4.655 chains/nm^2.

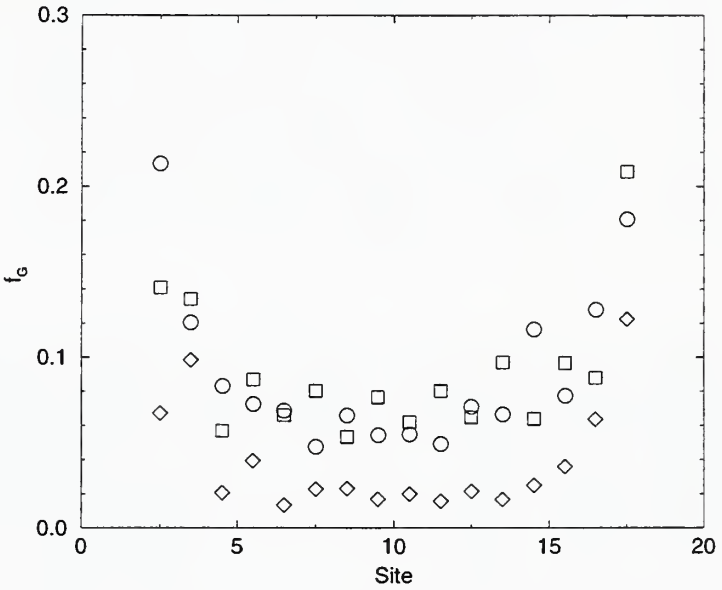

Figure 7. The average values for the faction of *gauche* defects is shown for the three cases. The diamonds are for C1, the squares are for C2, and the circles are for C3.

The order parameter S_2 for each site is shown in Fig. 8. The changes in the amount and type of order that occur as the packing density is decreased are evident from an examination of this figure. The S_2 order parameter appears to remain nearly uniform throughout the chains; *i. e.*, it is site-independent for all three packing densities and assumes its largest value of around 0.75 at the highest density. Loosely speaking, this implies that "orientational disorder" tends to be distributed uniformly along the chains rather than concentrated at the terminal methyl ends, an observation which is consistent with the distribution of *gauche* defects along the chains. The value of 0.75 for S_2 corresponds to a minimum "site tilt angle" of around 24°, which is practically identical to the sulfur-terminal methyl tilt angle of 26°. The approximate site-invariance of S_2 also implies that the set of vectors which connects alternating methylene groups is confined to the surface of a surface-normal cone whose apex is the terminal sulfur. The projection of these vectors onto the z-axis is practically constant along the alkane chain; *ie.*, statistically speaking, the chains are uniformly extended and "directed" perpendicular to the surface, and the overall "chain tilt" is determined by the spreading of this cone, which, because of symmetry considerations, must possess a circular cross-section.

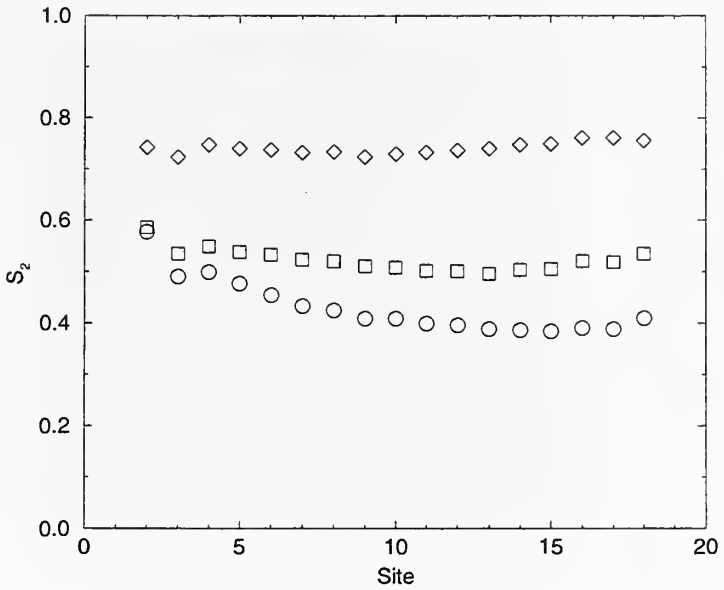

Figure 8. The order parameter, S_2 for the three cases with free translation are displayed. The diamonds are for C1, the squares are for C2, and the circles are for C3.

The density profiles indicate that at the highest density there is a high degree of spatial order on a site by site basis in the lower parts of the chains. This order becomes less pronounced in the upper parts of the chains, but is still visible. Also, the interface formed by the methyl sites of the membrane is fairly sharp, with a thickness of about 0.2 nm. This is consistent with the tilt angle distribution being concentrated around an angle of 26°. The density profiles for the C2 and C3 cases indicate that the spatial order is "lost" as the packing density decreases. In particular, the interface formed by the methyl sites becomes rather broad. This is reflected in the broad tilt angle distributions and in the changes that occur in f_G and in S_2 as the density decreases.

Some further insight into the ordering of the membranes can be obtained by examining snapshots of configurations rather than selected profiles and other statistically averaged properties. This approach is discussed in the following paragraphs. In Figs. 9–11, the methyl sites are the large, light gray features, the CH_2 sites are the small, darker features, and the thiol sites are small, black features which are usually masked out by the sites lying above them. These snapshots are views from above the membranes directed approximately downward along the z-axis.

The first system, C1, has a high density of 4.655 chains/nm^2, which is the close-packed density for the alkane thiols. This system maintains a high degree of order as is evident from the snapshot of one configuration shown in Fig. 9. The thiol sites (not visible) form into a hexagonal array as do the methyl sites at the free end of the chains. The chains develop a tilt of about 25° to 30° from the normal to the surface. The faction of *gauche* defects per chain is small, unlike the shorter chains at this density that develop a significant fraction of *gauche* defects per chain.[23]

The second system, C2, has a lower density of 3.605 chains/nm^2. There is some disorder

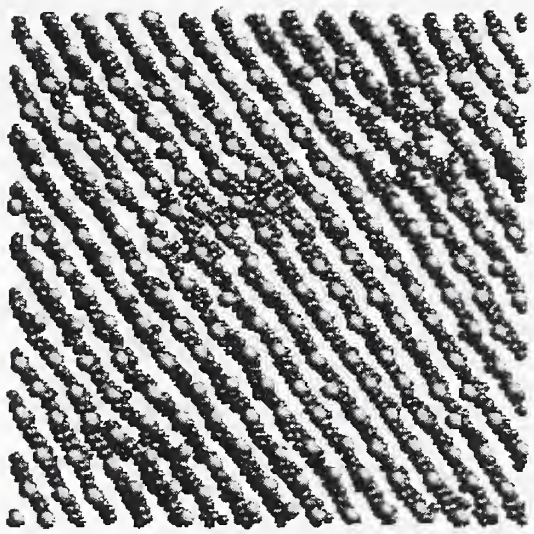

Figure 9. A snapshot of a configuration for C1.

present as can be seen in Fig. 10. The system appears to form hexagonally ordered domains, with considerable disorder between the domains. The chains in the ordered regions develop a tilt of about 35° from the normal to the surface and the chains in the disordered region have a wide range of tilt angles. The interface formed by the methyl sites is fairly sharp within the domains, but is broad and less well defined in the disordered regions.

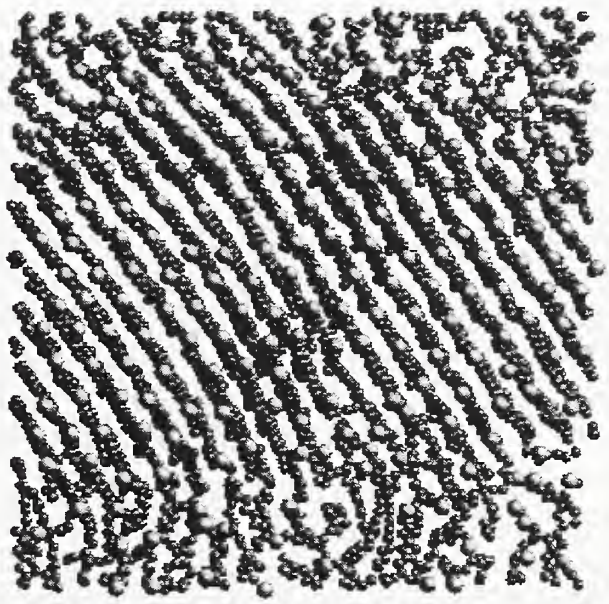

Figure 10. A snapshot of a configuration for C2.

The density of the third system, C3, is 2.504 chains/nm^2. The resulting structure displays some interesting features as may be seen in Fig. 11. There is a substantial region where the chains are ordered. There the methyl groups have a nearly hexagonal arrangement, much like the close packed system. There is also a region where the local density of chains is fairly low and the chains are "lying down" rather than upright relative to the tethering surface. This is consistent with the tilt angle distribution displayed in Fig. 6. There is a relatively narrow "interface" between these ordered and disordered regions.

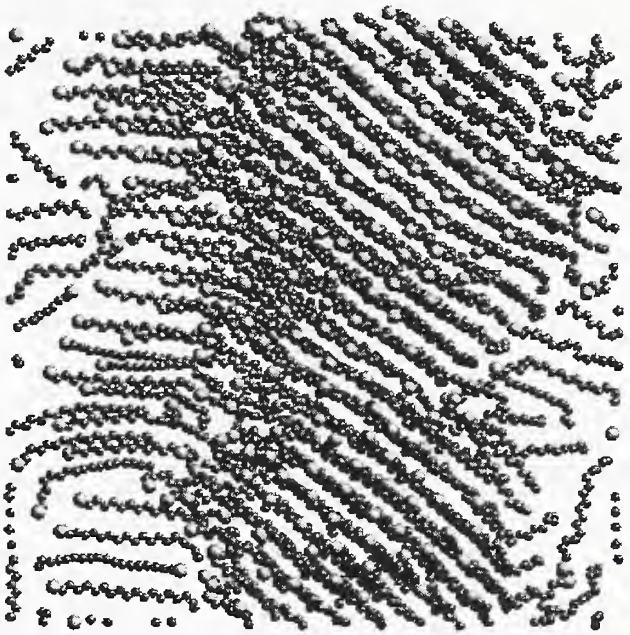

Figure 11. A snapshot of a configuration for C3.

4. Results, bound cases

Two additional cases at the lowest packing density were examined. These differed from the free translation case at the same density by the "random", fixed arrangement of the bonding sites. The bonding sites were not allowed to translate, as would be the case for tethered chain layers in RPLC columns.

Freezing in the initial configuration of the bonding sites has consequences for the type of membranes that result. In the following few figures, we compare results for the free translation, C3, and bound cases, C4 and C5. The density profiles differ primarily at the upper part of the membrane, as indicated in Fig. 12. There the profiles for C3 (dashed line) and for C4 (solid line) are displayed. The profile for C5 is not shown as it is quite close to that for C4. The bound case has a more diffuse surface than does the free translation case.

The tilt angle distributions of the bound cases are less structured than the distribution for the free translation case. This is indicated in Fig. 13. The solid line is for C4 and the dashed line is for C3. The distribution for C5 is very close to that for C4 and is not displayed. A comparison between the tilt angle distributions associated with the low

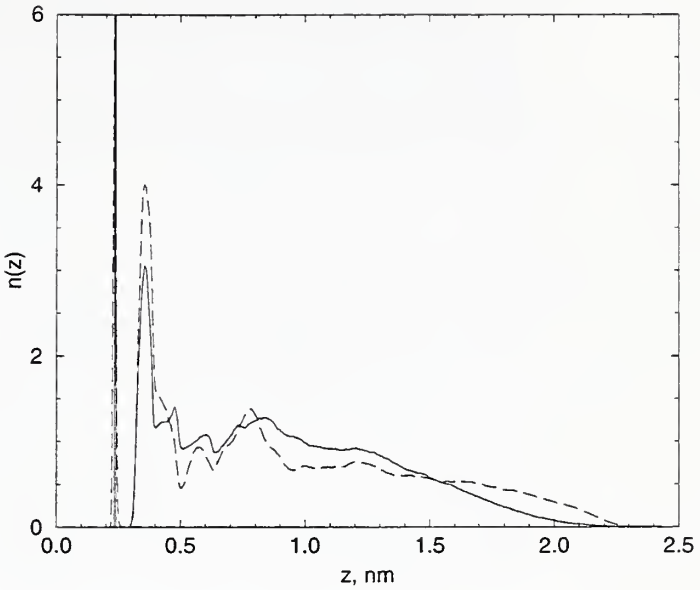

Figure 12. Density profiles for the "bound" C4 case, solid line, and for the "free" C3 case, dashed line, are shown as a function of z, the distance above the substrate.

density free translation case and the low density bound case indicates much more structure in the former distribution; this is a direct consequence of free translation chain clustering and overlap.

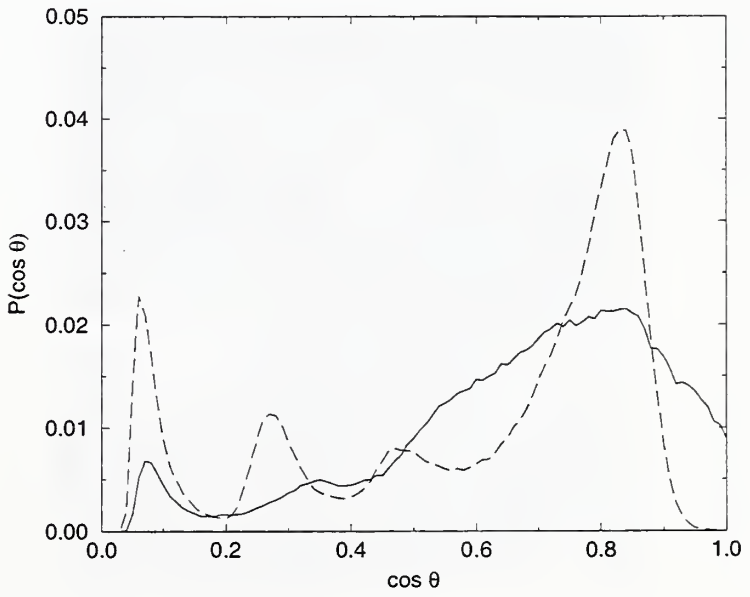

Figure 13. The tilt angle distribution for C4, solid line, and for C3, dashed line, are shown.

The amount of disorder in the chains, as measured by the fraction of *gauche* defects per site is higher for the bound cases than for the free translation case. This is indicated in

Fig. 14. The circles are for C4, the diamonds are for C5, and the squares are for C3. There is no significant difference in the amount of disorder in cases C4 and C5.

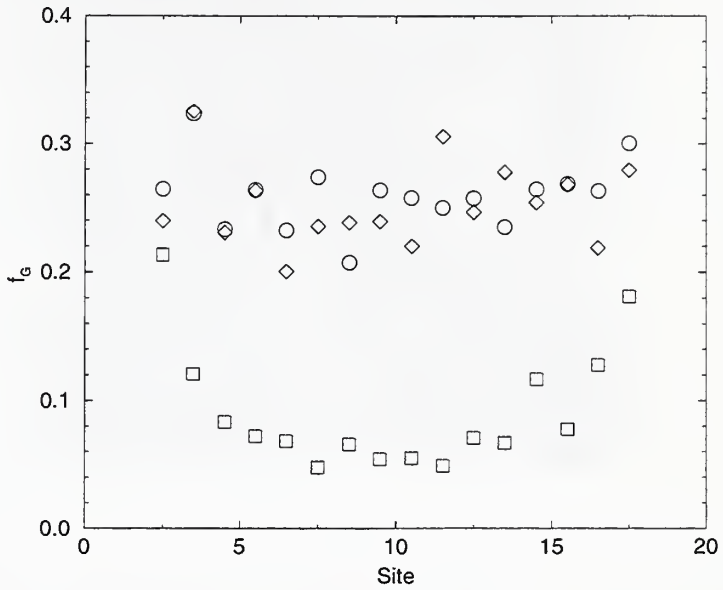

Figure 14. The fraction of defects per site is shown. The bound cases, circles and diamonds, have defects fairly uniformly distributed. The defects are mainly at the ends of the chains for the free translation case, squares.

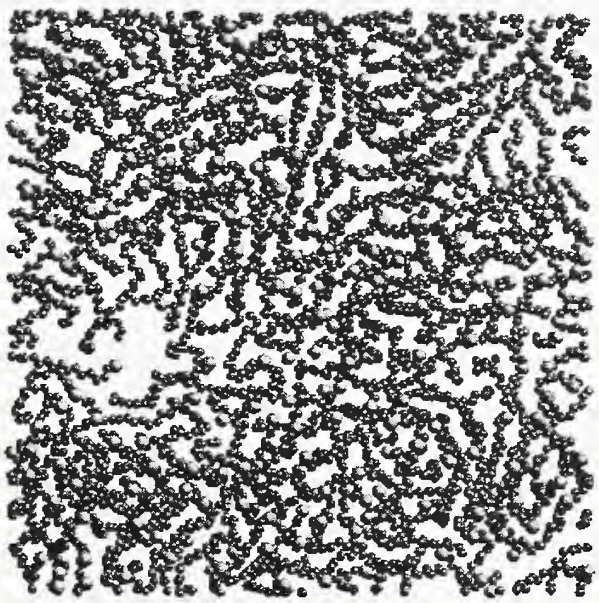

Figure 15. A snapshot of a configuration for C4.

Snapshots of the configurations of the bound cases are displayed in Figs. 15 and 16. Comparing these views with that of case C3 in Fig. 11 is quite instructive. When free translation

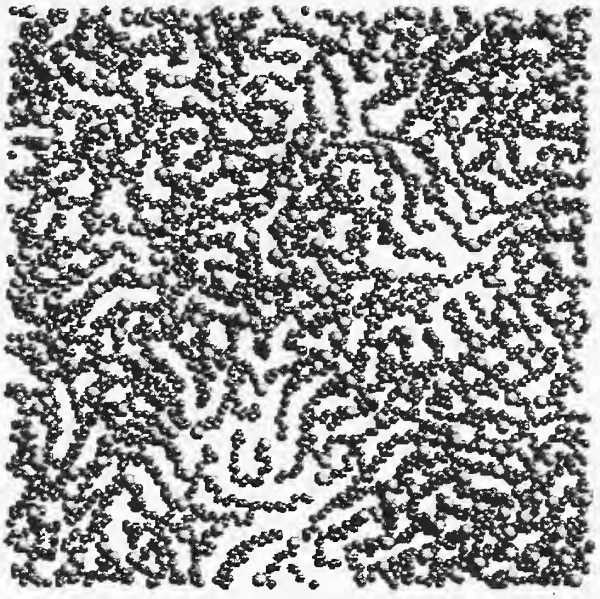

Figure 16. A snapshot of a configuration for C5.

is allowed, the chains tend to be arranged into dense, ordered regions and into coexisiting low density regions. In the low density regions, the chains are nearly horizontal resulting in the structure in $P(\cos\theta)$ for small values of $\cos\theta$. In the bound cases, the coverage is more uniform in the sense of a local density of chains. Also, the type of coverage is different in the two situations. Free translation leads to regions where lattice planes are present for intervals on the order of 10 chain spacings. No such regularity is evident in the bound cases. By comparing the fraction of *gauche* defects per site for surface bound chains with the fraction for free translation chains, one can conclude that strong chain-chain interactions (packing effects) promote ordering at each site, whereas strong surface interactions tend to induce site disorder by increasing the local fraction of *gauche* defects.

5. Discussion

Free translation cases

Our simulations match the experimental characterization from ellipsometry, electrochemistry, X-ray diffraction, scanning tunneling microscopy, and infrared spectroscopy for the high-density case. For example, we observe thicknesses of between 2.2 and 2.4 nm compared to values of 2.3 nm and 2.2 nm from ellipsometry and X-ray diffraction respectively. We observe small patches of thinner/disordered regions that are less blocking to electrochemistry as shown in Figure 9. Our angles for the tilt of the alkane chains agree with X-ray diffraction and infrared spectroscopy. In addition, infrared spectroscopy determinations of the concentration of terminal *gauche* conformers are consistent with the total fraction of *gauche* conformers we observe.

However, for 19-site chains it is difficult to measure specific information about the lower

density cases and so these are much less verified. The experimental characterization of these cases is compounded by the difficulty in repeatedly forming an experimental system with the desired packing density. In addition, most of the experimental methods used to characterize monolayers have difficulty discriminating between differences in the structure of the monolayer and differences in the number of chains present. In measuring thickness, ellipsometry, electrochemistry and X-ray diffraction assume the measured signal comes from a layer with uniform thickness and density. To separate contributions from parts of the layer with different thicknesses or densities, values for the contributing parts must be known to determine the amount of each present. These measurement difficulties make molecular dynamics simulations important tools for understanding the structures and properties of surface tethered chains.

Our molecular dynamics simulations, especially of the lower density cases, show a variety of structural features indicative of variations in the properties across the 225 chains sampled. For example, our simulations of freely translating chains clearly indicate the presence of highly ordered structures at near close packed densities as well as disordered configurations at lower surface densities. We find that the ability of the tethered chains to glide across the flat surface leads to the formation of tightly packed domains separated by relatively disordered "walls". This is in marked contrast to the situation in which the surface terminal groups are randomly localized without the possibility of chain overlap, thereby preventing domain formation via short ranged repulsive interactions. We therefore conclude that surface mobility and short-ranged interactions play key roles in domain formation for surface tethered alkane chains.

The uniformity of the S_2 order parameter distribution throughout the interiors of the chains, independent of surface density, is one of the more significant results of the simulation, and so it would be of interest to design an experimental test of this prediction. The marked contrast between the tilt angle distributions for the low density localized and de-localized simulations implies that the overlap of collapsed chains introduces significant orientation structured features, and it would be of interest to make a careful comparison with scanning-tunneling or atomic force microscopy studies of these systems.

Bound cases

When the chains are tethered to specific sites on the surface, the resulting film has rather different structure when compared with the film where the chains are free to translate along the surface. Given the way these films were generated, the overall density of chains is limited to perhaps 1/2 that possible when the chains are free to translate. This is because of the random placement of the tethering sites and the constraint of no overlap of the bonding sites of the chains.

The most striking difference is that there are no regions where the chains have the ordering noted in Fig. 11. Instead, as may be seen in Figs. 15 and 16, the appearance of the film is one of spatial disorder. Also, there are no extensive regions where the chains appear to be nearly horizontal with respect to the surface. It should be noted that the bound films have a more "uniform" appearance in these figures. This is also evident from the density profile comparison in Fig. 12. The bound chains have less structure in the film between

1 nm and 2 nm above the surface than do the freely translating chains. This is also seen in the orientation distributions shown in Fig. 13. The bound chains have less structure in this distribution and the more vertically oriented chains have a broader distribution of orientations when compared with the free translation case.

The bound film case presents an upper surface (the methyl groups) that is "rough" on the scale of a few molecular diameters. This is illustrated in Fig. 17 where a side view of the film of case C4 is displayed. The type of interface the bound film presents has a coarser structure than that provided by the free translation case. It *may be* that this type of structure is significant for the performance of Reversed Phase Liquid Chromatography, as the films employed in this separation process consist of relatively low surface densities of randomly arranged chains.[24, 25]

Figure 17. A snapshot of a configuration for C4 from one side rather than looking down.

References

[1] M. D. Porter, T. B. Bright, D. L. Allara, and C. E. Chidsey, "Spontaneously organized molecular assemblies. 4. Structural characterization of n-alkyl thiol monolayers on gold by optical ellipsometry, infrared spectroscopy , and electrochemistry," *J. Am. Chem. Soc.*, vol. 109, pp. 3559–3568, 1987.

[2] R. W. Collins, D. L. Allera, Y.-K. Kim, Y. Lu, and J. Shi, in *Characterization of Organic Thin Films*, edited by A. Ulman, Butterworth-Heineman, Boston, pp. 48–49, 1995.

[3] C. E. D. Chidsey and D. N. Loiacono, "Chemical and functionality in self-assembled monolayers: Structural and electrochemical properties," *Langmuir*, vol. 6, pp. 682–691, 1990.

[4] L. Strong and G. M. Whitesides, "Structures of self-assembled monolayer films of organosulfur compounds adsorbed on gold single crystals; electron diffraction studies," *Langmuir*, vol. 4, pp. 546–558, 1988.

[5] N. Camillone III, C. E. D. Chidsey, G.-Y. Liu, and G. Scoles, "Superlattice structure at the surface of a monolayer of octadecanethiol self- assembled on Au(111)," *J. Chem. Phys.*, vol. 98, pp. 3505–3511, 1993.

[6] G. E. Poirier, "Characterization of Organosulfur Molecular Monolayers on Au(111) using Scanning Tunneling Microscopy," *Chem. Rev.*, vol. 97, pp. 1117–1127, 1997.

[7] P. E. Labinis, G. M. Whitesides, D. L. Allara, Y.-T. Tao, A. N. Parikh, and G. G. Nuzzo, "Comparison of the structures and wetting properties of self-assembled monolayers of n-alkanethiols on the coinage metal surfaces, Cu, Ag, Au," *J. Am. Chem. Soc.*, vol. 113, pp. 7152–7167, 1991.

[8] A. N. Parikh and D. L. Allara, "Quantitative determination of the molecular structure in multilayered and thin films of biaxial and lower symmetry from photon spectroscopies. I. Reflection infrared vibrational spectroscopy," *J. Chem. Phys.*, vol. 96, pp. 927–945, 1992.

[9] L. H. Dubois, B. R. Zegarski, and R. G. Nuzzo, "Molecular ordering of organosulfur compounds on Au(111) and Au(100): Adsorption from solution and in ultrahigh vacuum," *J. Chem. Phys.*, vol. 98, pp. 678–688, 1993.

[10] P. Fenter, P. Eisenberger, and K. S. Liang, "Chain-length dependence of the structure and phases of $CH_3(CH_2)_{n-1}SH$ self assembled on Au(111)," *Phys. Rev. Lett.*, vol. 70, pp. 2447–2450, 1993.

[11] N. Camillone III, C. E. D. Chidsey, P. Fenter, J. Li, K. S. Liang, G.-Y. Liu, and G. J. Scoles, "Structural defects in self-assembled organic monolayers via combined atomic beam and x-ray diffraction," *J. Chem. Phys.*, vol. 99, pp. 744–747, 1993.

[12] R. H. Terrill, T. A. Tanzer, and P. W. Bohn, "Structural evolution of hexadecanethiol monolayers on gold during assembly: Substrate and concentration dependence of monolayer structure and crystallinity," *Langmuir*, vol. 14, pp. 845–855, 1998.

[13] C. W. Meuse, J. T. Connor, L. J. Richter, and A. L. Plant, "Quantitative analysis of the molecular structure of thin films using infrared reflection spectroscopy," *Applied Spectroscopy*, 2000, Submitted for publication.

[14] J. Hautman and M. L. Klein, "Simulation of a monolayer of akyl thiol chains," *J. Chem. Phys.*, vol. 91, pp. 4994–5001, 1989.

[15] J. H. Hautman and M. L. Klein, "Molecular dynamics simulation of the effects of temperature on a dense monolayer of long- chain molecules," *J. Chem. Phys.*, vol. 93, pp. 7483–7492, 1990.

[16] G. E. Poirier and M. J. Tarlov, "The c(4x2) Superlattice on n-Alkanethiol Monolayers Self-Assembled on Au(111)," *Langmuir*, vol. 10, pp. 2853–2856, 1994.

[17] G. E. Poirier, M. J. Tarlov, and H. E. Rushmeier, "Two-Dimensional Liquid Phase and the p x $\sqrt{3}$ Phase of Alkanethiol Self-Assembled Monolayers on Au(111)," *Langmuir*, pp. 3383–3386, 1994.

[18] W. Mar and M. L. Klein, "Molecular Dynamics Study of the Self-Assembled Monolayer Composed of $S(CH_2)_{14}$ Molecules Using an All-Atoms Model," *Langmuir*, vol. 10, pp. 188–196, 1994.

[19] B. Smit, S. Karaborni, and J. I. Siepmann, "Computer simulations of vapor-liquid equilibria of *n*-alkanes," *J. Chem. Phys.*, vol. 102, pp. 2126–2140, 1995.

[20] J. H. R. Clarke and D. Brown, "Molecular dynamics computer simulation of chain molecule liquids I. The coupling of torsional motions to translational diffusion," *Mol. Phys.*, vol. 58, pp. 815–825, 1986.

[21] J. Hautman, J. P. Bareman, W. Mar, and M. L. Klein, "Molecular Dynamics Investigations of Self-assembled Monolayers," *J. Chem. Soc. Faraday Trans.*, vol. 87, pp. 2031–2037, 1991.

[22] R. D. Mountain and A. C. Brown, "Molecular dynamics study of the liquid and plastic phases of neopentane," *J. Chem. Phys.*, vol. 82, pp. 4236–4242, 1985.

[23] R. D. Mountain and J. B. Hubbard, "Molecular Dynamics Simulation of Tethered Chains," NISTIR 6150, National Institute of Standards and Technology, 1998.

[24] L. C. Sander, C. J. Glinka, and S. A. Wise, "Determination of Bonded Phase Thickness in Liquid Chromatography by Small Angle Neutron Scattering," *Anal. Chemistry*, vol. 62, pp. 1099–1101, 1990.

[25] C. J. Glinka, L. C. Sander, S. A. Wise, and N. F. Berk, "Characterization of Chemically Modified Pore Surfaces by Small Angle Neutron Scattering," in *Materials Research Society Symposium Proceedings Volume 166*, 1990, pp. 415–420.

Appendix, Model parameters

The model potential parameters are listed in this appendix.

Table 1. Stretch parameters. The CH_3 and CH_2 sites are equivalent for the stretch interaction.

Parameter	S-C	C-C
γ_2, 10^7 K/nm^2	4.529	4.529
d_0, Å	1.82	1.54

Table 2. Bend parameters.

Parameter	C-C-C	S-C-C
γ_θ, 10^3K/rad^2	62.5	62.5
θ_0, deg	109.5	114.4

Table 3. The coefficients, C_l, in the torsional potential.[20] Note that there is no site dependence for these coefficients

l	C_l, K
0	1116
1	1462
2	-1578
3	-368
4	3156
5	-3788

Table 4. The parameters for the surface interactions.[14]

Site	C_{12}, 10^7KÅ^{12}	C_3, KÅ^3	z_0, Å
CH_3	3.41	20800	0.860
CH_2	2.80	17100	0.860
S	4.089	180600	0.269

Table 5. Lennard-Jones parameters.

Sites	σ, Å	ϵ, K
S_I-S_I	4.25	200.
CH_3-CH_3	3.905	88.1
CH_2-CH_2	3.905	59.4
CH_3-CH_2	3.905	72.3
CH_3-S	3.723	105.4
CH_2-S	3.723	86.5